# Effects of crystallinity and point defects on optoelectronic applications of β-$Ga_2O_3$ epilayers

**Parvaneh Ravadgar,[1] Ray-Hua Horng,[1,2,*] Shu-De Yao,[3] Hsin-Ying Lee,[1] Bing-Rui Wu,[4] Sin-Liang Ou,[4] and Li-Wei Tu[5]**

[1]*Department of Photonics and Advanced Optoelectronic Technology Center, National Cheng Kung University, No. 1, University Road, Tainan 70101, Taiwan*

[2]*Graduate Institute of Precision Engineering, National Chung Hsing University, 250 Kuo Kuang Road, Taichung 40227, Taiwan*

[3]*State Key Laboratory of Nuclear Physics and Technology, Peking University, 5 Yiheyuan Road, Haidian District, Beijing, 100871, China*

[4]*Department of Materials Science and Engineering, National Cheng Kung University, No. 1, University Road, Tainan 70101, Taiwan*

[5]*Department of Physics and Center for Nanoscience and Nanotechnology, National Sun Yat-Sen University, 70 Lienhai Road, Kaohsiung 80424, Taiwan*

[*]*huahorng@nchu.edu.tw*

**Abstract:** This study evaluates the effect of crystallinity and point defects on time-dependent photoresponsivity and the cathodoluminescence (CL) properties of β-$Ga_2O_3$ epilayers. A synchrotron high-resolution X-ray technique was used to understand the crystalline structure of samples. Rutherford backscattering spectroscopy was used to determine the net chemical composition of the samples to examine the type and ratio of their possible point defects. The results show that in functional time-dependent photoresponsivity of photodetectors based on β-$Ga_2O_3$ epilayers, point defects contribution overcomes the contribution of crystallinity. However, the crystalline structure affects the intensities and emission regions of CL spectra more than point defects.



**OCIS codes:** (250.0250) Optoelectronics; (310.0310) Thin films.

## References and links

1. M. Yoshimoto, T. Maeda, T. Ohnishi, H. Koinuma, O. Ishiyama, M. Shinohara, M. Kubo, R. Miura, and A. Miyamoto, "Atomic-scale formation of ultrasmooth surfaces on sapphire substrates for high-quality thin-film fabrication," Appl. Phys. Lett. **67**(18), 2615–2617 (1995).
2. K. Nomura, H. Ohta, K. Ueda, T. Kamiya, M. Hirano, and H. Hosono, "Thin-film transistor fabricated in single-crystalline transparent oxide semiconductor," Science **300**(5623), 1269–1272 (2003).
3. M. H. Huang, S. Mao, H. Feick, H. Yan, Y. Wu, H. Kind, E. Weber, R. Russo, and P. Yang, "Room-temperature ultraviolet nanowire nanolasers," Science **292**(5523), 1897–1899 (2001).
4. C. Y. Su, A. Y. Lu, Y. Xu, F. R. Chen, A. N. Khlobystov, and L. J. Li, "High-quality thin graphene films from fast electrochemical exfoliation," ACS Nano **5**(3), 2332–2339 (2011).
5. M. Barhoum, J. M. Morrill, D. Riassetto, and M. H. Bartl, "Rapid sol-gel fabrication of high-quality thin-film stacks on planar and curved substrates," Chem. Mater. **23**(23), 5177–5184 (2011).
6. M. S. Su, C. Y. Kuo, M. C. Yuan, U. S. Jeng, C. J. Su, and K. H. Wei, "Improving device efficiency of polymer/fullerene bulk heterojunction solar cells through enhanced crystallinity and reduced grain boundaries induced by solvent additives," Adv. Mater. **23**(29), 3315–3319 (2011).
7. Y. Hu, Y. Q. Chen, Y. C. Wu, M. J. Wang, G. J. Fang, C. Q. He, and S. J. Wang, "Structural, defect and optical properties of ZnO films grown under various $O_2$/Ar gas ratios," Appl. Surf. Sci. **255**(22), 9279–9284 (2009).
8. L. Hu, L. Wu, M. Liao, and X. Fang, "High-performance $NiCo_2O_4$ nanofilm photodetectors fabricated by an interfacial self-assembly strategy," Adv. Mater. **23**(17), 1988–1992 (2011).
9. T. Y. Zhai, X. S. Fang, M. Y. Liao, X. J. Xu, L. Li, B. D. Liu, Y. Koide, Y. Ma, J. N. Yao, Y. Bando, and D. Golberg, "Fabrication of high-quality $In_2Se_3$ nanowire arrays toward high-performance visible-light photodetectors," ACS Nano **4**(3), 1596–1602 (2010).
10. H. K. Yadav, K. Sreenivas, and V. Gupta, "Study of metal/ZnO based thin film ultraviolet photodetectors: The effect of induced charges on the dynamics of photoconductivity relaxation," J. Appl. Phys. **107**(4), 044507 (2010).

#196199 - $15.00 USD Received 21 Aug 2013; revised 27 Sep 2013; accepted 30 Sep 2013; published 7 Oct 2013

11. X. Xie, S.-Y. Kwok, Z. Lu, Y. Liu, Y. Cao, L. Luo, J. A. Zapien, I. Bello, C.-S. Lee, S.-T. Lee, and W. Zhang, "Visible-NIR photodetectors based on CdTe nanoribbons," Nanoscale **4**(9), 2914–2919 (2012).
12. M. Chen, C. Ye, S. Zhou, and L. Wu, "Recent advances in applications and performance of inorganic hollow spheres in some devices," Adv. Mater. (to be published).
13. W. Y. Weng, T. J. Hsueh, S. J. Chang, G. J. Huang, and H. T. Hsueh, "A β-$Ga_2O_3$ solar-blind photodetector prepared by furnace oxidization of GaN thin film," IEEE Sens. J. **11**(4), 999–1003 (2011).
14. K. Wang, F. Chen, N. Allec, and K. S. Karim, "Fast lateral amorphous-selenium metal–semiconductor–metal photodetector with high blue-to-ultraviolet responsivity," IEEE Trans. Electron. Dev. **57**(8), 1953–1958 (2010).
15. M. M. Cao, R. J. Chacon, and C. E. Hunt, "A field emission light source using a reticulated vitreous carbon (RVC) cathode and cathodoluminescent phosphors," J. Disp. Technol. **7**(9), 467–472 (2011).
16. P. Ravadgar, R. H. Horng, and T. Y. Wang, "Healing of surface states and point defects in single-crystalline β-$Ga_2O_3$ epilayer," ECS J. Solid State Sci. Technol. **1**(4), N58–N60 (2012).
17. P. Ravadgar, R. H. Horng, and S. L. Ou, "A visualization of threading dislocations formation and dynamics in mosaic growth of GaN-based light emitting diode epitaxial layers on (0001) sapphire," Appl. Phys. Lett. **101**(23), 231911 (2012).
18. P. Erhart, A. Klein, and K. Albe, "First-principles study of the structure and stability of oxygen defects in zinc oxide," Phys. Rev. B **72**(8), 085213 (2005).
19. J. F. Scott and M. Dawber, "Oxygen-vacancy ordering as a fatigue mechanism in perovskite ferroelectrics," Appl. Phys. Lett. **76**(25), 3801–3803 (2000).
20. A. S. Foster, V. B. Sulimov, F. L. Gejo, A. L. Shluger, and R. N. Nieminen, "Structure and electrical levels of point defects in monoclinic zirconia," Phys. Rev. B **64**(22), 224108 (2001).
21. A. S. Foster, F. L. Gejo, A. L. Shluger, and R. M. Nieminen, "Vacancy and interstitial defects in hafnia," Phys. Rev. B **65**(17), 174117 (2002).
22. J. B. Varley, J. R. Weber, A. Janotti, and C. G. Van de Walle, "Oxygen vacancies and donor impurities in β-$Ga_2O_3$," Appl. Phys. Lett. **97**(14), 142106 (2010).
23. F. Devynck, M. Iannuzzi, and M. Krack, "Frenkel pair recombinations in $UO_2$: Importance of explicit description of polarizability in core-shell molecular dynamics simulations," Phys. Rev. B **85**(18), 184103 (2012).
24. B. J. Morgan and P. A. Madden, "Effects of lattice polarity on interfacial space charges and defect disorder in ionically conducting AgI heterostructures," Phys. Rev. Lett. **107**(20), 206102 (2011).
25. J. P. Crocombette, D. Torumba, and A. Chartier, "Charge states of point defects in uranium oxide calculated with a local hybrid functional for correlated electrons," Phys. Rev. B **83**(18), 184107 (2011).
26. Z. L. Wang, J. S. Yin, and Y. D. Jiang, "EELS analysis of cation valence states and oxygen vacancies in magnetic oxides," Micron **31**(5), 571–580 (2000).
27. A. Linsebigler, G. Lu, and J. T. Yates, "CO chemisorption on $TiO_2$(110): Oxygen vacancy site influence on CO adsorption," J. Chem. Phys. **103**(21), 9438–9443 (1995).
28. J. Hao and M. Cocivera, "Optical and luminescent properties of undoped and rare-earth-doped $Ga_2O_3$ thin films deposited by spray pyrolysis," J. Phys. D Appl. Phys. **35**(5), 433–438 (2002).
29. C. H. Liang, G. W. Meng, G. Z. Wang, Y. W. Wang, L. D. Zhang, and S. Y. Zhang, "Catalytic synthesis and photoluminescence of β-$Ga_2O_3$ nanowires," Appl. Phys. Lett. **78**(21), 3202–3204 (2001).
30. S. C. Vanithakumari and K. K. Nanda, "A one-step method for the growth of $Ga_2O_3$-nanorod-based white-light-emitting phosphors," Adv. Mater. **21**(35), 3581–3584 (2009).
31. D. M. Duffy, J. P. Hoare, and P. W. Tasker, "Vacancy formation energies near the surface of an ionic crystal," J. Phys. C Solid State Phys. **17**(7), L195–L199 (1984).
32. W. Tian, C. Y. Zhi, T. Y. Zhai, S. M. Chen, X. Wang, M. Y. Liao, D. Golberg, and Y. Bando, "In-doped $Ga_2O_3$ nanobelt based photodetector with high sensitivity and wide-range photoresponse," J. Mater. Chem. **22**(34), 17984–17991 (2012).
33. W. Tian, C. Y. Zhi, T. Y. Zhai, X. Wang, M. Y. Liao, S. L. Li, S. M. Chen, D. Golberg, and Y. Bando, "Ultrahigh quantum efficiency of CuO nanoparticle decorated $In_2Ge_2O_7$ nanobelt deep-ultraviolet photodetectors," Nanoscale **4**(20), 6318–6324 (2012).
34. Y. B. Li, T. Tokizono, M. Y. Liao, M. Zhong, Y. Koide, I. Yamada, and J. J. Delaunay, "Efficient assembly of bridged β-$Ga_2O_3$ nanowires for solar-blind photodetection," Adv. Funct. Mater. **20**(22), 3972–3978 (2010).
35. T. C. Lovejoy, R. Chen, X. Zheng, E. G. Villora, K. Shimamura, H. Yoshikawa, Y. Yamashita, S. Ueda, K. Kobayashi, S. T. Dunham, F. S. Ohuchi, and M. A. Olmstead, "Band bending and surface defects in β-$Ga_2O_3$," Appl. Phys. Lett. **100**(18), 181602 (2012).

## 1. Introduction

Good quality crystal refers to the new materials grown by using different techniques for different applications [1–5]. This study applies this concept to optoelectronic applications by examining monoclinic gallium oxide (β-$Ga_2O_3$) epilayers before and after post-annealing. Crystallinity and point defects reflect the quality of a single crystal. Crystallinity and point defects contribute differently to the optoelectronic properties of devices [6, 7]. This study qualitatively examines these contributions. Time-dependent photoresponsivity and cathodoluminescence (CL) spectroscopy are two powerful and common techniques, therefore they were used to understand the optoelectronic properties of β-$Ga_2O_3$ epilayers.

#196199 - $15.00 USD Received 21 Aug 2013; revised 27 Sep 2013; accepted 30 Sep 2013; published 7 Oct 2013

Time-dependent photoresponsivity is a fundamental parameter of optoelectronic technology. It determines the capability of a detector to follow rapidly varying optical signals [8]. Time-dependent photoresponsivity is also widely accepted as a qualified common reaction of materials that is used to confirm their degree of crystallinity [9] and the presence of point defects [10]. Many studies have used the advantages of fast photoresponsivity to test the quality (crystallinity) of their materials [11, 12]. However, some materials exhibit low crystallinity and fast photoresponsivity [13, 14]. The current hypotheses cannot explain this.

CL spectroscopy measures the photon emission from a specimen stimulated by an electron beam. It allows wide bandgap materials to be studied [15]. Although different science and technology fields (such as geology, mineralogy, materials science, and fundamental experimental physics) use CL spectroscopy for many applications, its origins and mechanism are unclear.

β-$Ga_2O_3$ grown by a modified metal-organic chemical vapor deposition (MOCVD) maintains its crystalline structure up to a post-annealing temperature of 800 °C, but, exhibits a large reduction in its point defect density [16]. Therefore, MOCVD-grown β-$Ga_2O_3$ provides an excellent opportunity for observing the simultaneous effects of crystallinity and point defects on the optoelectronic applications of β-$Ga_2O_3$ epilayers. The crystalline structure of β-$Ga_2O_3$ converts at a post-annealing temperature of 900 °C. This provides another opportunity to study the effect of crystalline structure conversion on certain aspects of the optoelectronic applications of materials. This investigation experimentally demonstrates that some optoelectronic applications of the same material are more sensitive to crystallinity and some are more sensitive to point defects. This study aims to clarify meaning of good quality when applied to materials used for different optoelectronic applications.

## 2. Experiment

Modified MOCVD was used to grow 220-nm-thick β-$Ga_2O_3$ epilayers on sapphire substrates by using trimethylgallium and pure oxygen (99.999%) as precursors. Reference [24] described the process required to grow β-$Ga_2O_3$ epilayers. Some of the as-grown samples were post-annealed in air at 700 °C, 800 °C, and 900 °C for 30 min. To evaluate the crystalline structure and degree of crystallinity of the samples a synchrotron high-resolution X-ray diffraction (HR-XRD) system was implemented by using a wiggler beamline (BL17B1) from Shanghai Synchrotron Radiation Facility. A field-emission scanning electron microscope (FE-SEM) was used to examine the growth mode and morphology of the sample crystalline damage. To observe the cross-sectional damage morphology of the epilayers, samples were manually prepared and only a mechanical force was applied to avoid chemical contamination or other types of damage or effects from the cutting process. Rutherford backscattering spectroscopy **(**RBS) was conducted on the 5SDH-2 tandem accelerator at Peking University to determine the chemical composition of samples. Rump software was used to simulate and transact the RBS data. High-resolution transmission electron microscopy (HR-TEM, model: JEM-2100 F) was used to study point defects. The time-dependent photoresponsivity of the β-$Ga_2O_3$ epilayers before and after post-annealing was investigated by fabricating metal-semiconductor-metal (MSM) photodetectors (PDs) onto the epilayers. For fabrication of MSM PDs, Ni/Au (50/100 nm) film was deposited on samples by using e-beam evaporation to be served as Schottky contact metal. Standard photolithography and wet etching were used to make 2 × 2.2 $mm^2$ devices with interdigitated-shaped contact electrodes. The finger width and interspacing of the electrodes were the same and 100 μm (shown in Fig. 1). Time-dependent photoresponsivity was measured at room temperature by switching a 240-nm exciting light, with 1.035 × $10^{-8}$ W power at a bias voltage of 5 V, on and off 7 time times. A JOBIN-YVON SPEX system with a 300 W xenon arc lamp light source (PERKINELMER PE300BUV) was employed to measure time-dependent photoresponsivity of PDs. The luminescence properties of samples were explored by using a CL spectroscope.

#196199 - $15.00 USD Received 21 Aug 2013; revised 27 Sep 2013; accepted 30 Sep 2013; published 7 Oct 2013

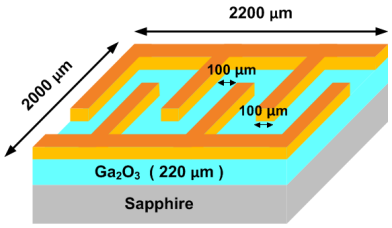


Fig. 1. Schematic diagram of a PD based on a β-$Ga_2O_3$ epilayer.

## 3. Data and analysis

### *3.1 Synchrotron HR-XRD*

The synchrotron HR-XRD patterns of typical samples in Fig. 2(a) show the formation of β-$Ga_2O_3$. The dominant orientation of (–402) for the first 3 epilayers is parallel to the growth direction. The presence of directions (401) and (–601) (indexed to β-$Ga_2O_3$), indicates the formation of crystalline impurity grains. This is different to the approach on the formation of pure single-crystalline β-$Ga_2O_3$ [16]. This is because the wavelength (λ) of the synchrotron X-ray (λ = 0.0688 nm) enables higher resolution analysis. Reference 24 used a higher wavelength X-ray with Cu $K_\alpha$ (λ = 0.1542 nm) as the radiation source. Post-annealed β-$Ga_2O_3$ epilayers at 700 °C and 800 °C exhibit the same crystalline structures as as-grown samples. Figure 2(a) shows that the disintegration of (–402) and the reconstruction of the (401) crystalline direction is the preferred orientation for a typical 900 °C-annealed β-$Ga_2O_3$ epilayers. The full width at half maximums (FWHMs) of each X-ray rocking curve pattern for typical as-grown and 700 °C and 800 °C-annealed samples in Fig. 2(b) are 0.0251°, 0.0340°, and 0.0319°, respectively. The synchrotron HR-XRD results shows that the (–402) crystalline direction produces the highest degree of crystallinity in as-grown sample. The degree of crystallinity finds its lowest value in 700 °C-annealed sample. The (–402) crystallinity direction disappears in 900 °C-annealed samples, confirming the results in Fig. 2(a).

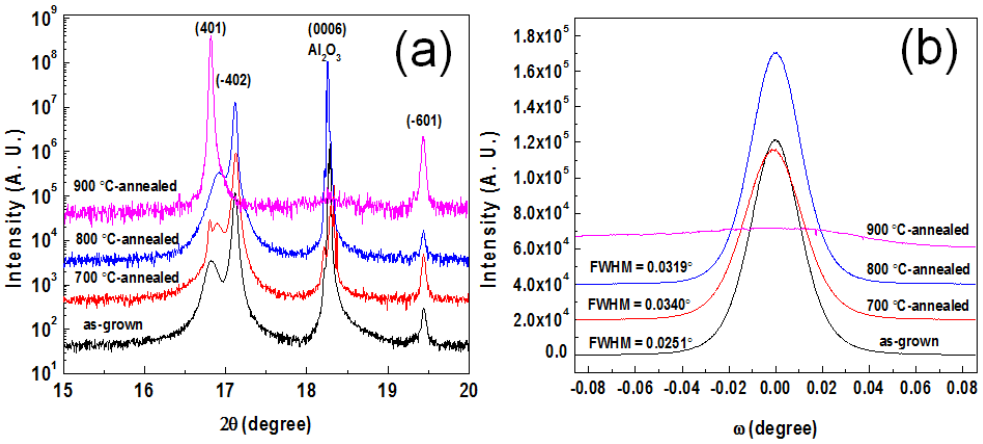


Fig. 2. Structural characterization of β-$Ga_2O_3$ epilayers on sapphire ($Al_2O_3$) substrates. (a) Synchrotron HR-XRD patterns for typical as-grown and 700 °C, 800 °C, and 900 °C-annealed samples. (b) Synchrotron x-ray rocking curve patterns for (–402) diffraction peaks of samples.

### *3.2 Surface morphologies*

Figures 3(a)–3(d) show FE-SEM top-view images of β-$Ga_2O_3$ epilayers. The top-view image of a typical as-grown sample in Fig. 3(a) shows many unfilled areas, which are absent in the post-annealed samples in Figs. 3(b)–3(d). Many parameters of the modified MOCVD system

#196199 - $15.00 USD Received 21 Aug 2013; revised 27 Sep 2013; accepted 30 Sep 2013; published 7 Oct 2013

were tuned to produce high quality (uniform thickness with the highest crystallinity) β-$Ga_2O_3$ epilayers, however unfilled areas were always observed. Internal stress of the materials cause these unfilled areas. The absence of unfilled areas in the post-annealed samples could be attributed to the disappearance of the source of the stress. The grains on the surface of the as-grown samples predict their mosaic growth mode. The size of a typical surface grain was approximately 100 nm, as shown in Fig. 3(a).

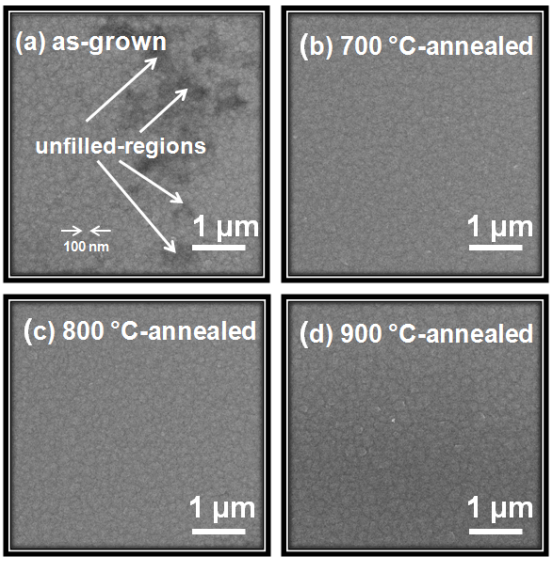


Fig. 3. Top-view FE-SEM images of (a) as-grown, (b) 700 °C, (c) 800 °C, and (d) 900 °C-annealed β-$Ga_2O_3$ epilayers.

*3.3 Cross-sectional morphologies*

Figures 4(a)–4(d) show cross-sectional FE-SEM images of typical β-$Ga_2O_3$ epilayers before and after post-annealing. The cross-section of the as-grown β-$Ga_2O_3$ epilayer in Fig. 4(a) shows many highly packed extended grains in the growth direction (–402), suggesting that the growth mode is the mosaic model [17]. Extended grains in the as-grown sample are smooth with few fractures along them. To better observe and compare the fractures in the extended grains of the first 3 samples with the same structure, magnified cross-sectional images are displayed in their insets. Extended grains with approximately 10 nm width are different to the surface grains, which are approximately 100 nm width. Figures 4(b) and 4(c) show that the highly packed grains in the 700 °C and 800 °C-annealed samples also extend in the same direction (–402) as the as-grown samples. The number density of fractures along with each extended grain in Fig. 4(b) is higher than in Fig. 4(a) and lower than in Fig. 4(c). Extended grains parallel with growth direction are disappeared in 900 °C-annealed sample (Fig. 4(d)). Many large fractures in the 900 °C-annealed sample are visible. These could be a result of re-crystallization.

#196199 - $15.00 USD Received 21 Aug 2013; revised 27 Sep 2013; accepted 30 Sep 2013; published 7 Oct 2013

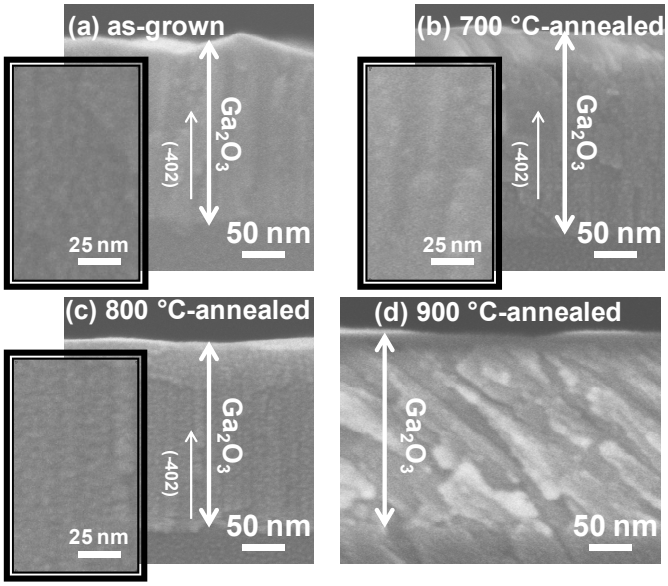


Fig. 4. Cross-sectional FE-SEM images of (a) as-grown, (b) 700 °C, (c) 800 °C, and (d) 900 °C-annealed β-$Ga_2O_3$ epilayers.

*3.4 TEM study*

Figures 5(a)–5(d) show cross-sectional HR-TEM images of the samples. Due to the very similar structures of both 700 °C and 800 °C-annealed samples measured by synchrotron HR-XRD, only the 800 °C-annealed sample was selected for HR-TEM study. The d-spacings of 4.82 Å and 4.7 Å are obtained from the line profile study of as-grown (Fig. 5(a)) and 800 °C-annealed (Fig. 5(b)) samples. They correspond to β-$Ga_2O_3$ (–201) plane with the standard d-spacing of 4.67 Å. The d-spacing of 2.37 Å was deduced from 900 °C-annealed sample (Fig. 5(c)), corresponding to the β-$Ga_2O_3$ (401) plane.

A magnified HR-TEM image of a typical region in the as-grown sample is presented in Fig. 5(d). Orientationally-ordered self-interstitials are clear in the image which are predicted in the previous hypotheses [18, 19]. Dumbbell-shaped structures were found in the entire region of the HR-TEM image of the as-grown sample. The highlighted dumbbell-interstitials in Fig. 5(d) are explained by a schematic diagram in Fig. 5(e).

Figure 5(e) shows a schematic diagram of two successive atomic rows in a crystal, each including two types of atoms. Successive orientationally-ordered vacancies of only one kind of atoms in one row are shown. The missing atoms have occupied other planes of the crystal. It is already predicted that point defects induce an effective electrical charge in their positions [20–22]. Therefore, vacancies attract the nearest atoms of the same type in their neighboring row to form orientationally-ordered self-interstitials. These attractions minimize the effective electrical charges of vacancies. This model presents Frenkel pairs [23, 24]. The diagram clearly demonstrates that Frenkel pairs persuade zero net charge [25]. Therefore, stoichiometric ratio measurement is unable to reveal Frenkel pairs, because there are no net vacancies or interstitials. Self-interstitials are sometimes referred to dumbbell-interstitials for the symmetry around the shared atoms [18]. The high stress attributed to the local electric fields of orientationally-ordered self-interstitials could be responsible for unfilled regions in Fig. 3(a). The 800 °C and 900 °C-annealed samples do not show any dumbbell-interstitial. Probably, post-annealing has provided enough energy for the Frenkel pairs to find and repair each other. Moreover, immigration of Frenkel pairs during the annealing could be the origin of fractures in Figs. 4(a)–4(c). Later in another study, we will evaluate the mechanism of orientationally-ordered self-interstitials in more detail.

#196199 - $15.00 USD Received 21 Aug 2013; revised 27 Sep 2013; accepted 30 Sep 2013; published 7 Oct 2013

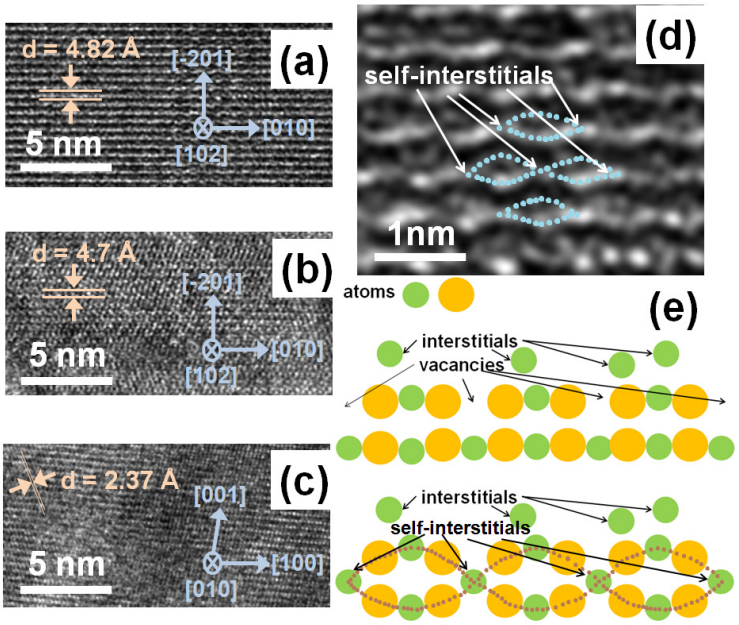


Fig. 5. HR-TEM images of typical (a) as-grown and (b) 800 °C and (c) 900 °C-annealed β-$Ga_2O_3$ epilayers. (d) A magnified typical region of an HR-TEM image of the as-grown sample. (e) A schematic diagram to explain the orientationally-ordered self-interstitials in the as-grown sample.

### *3.5. Atomic composition*

In β-$Ga_2O_3$ epilayers, the atomic composition varies as the post-annealing temperature changes (Table 1). These results indicate an almost ideal stoichiometric ratio for the 700 °C-annealed samples. No net vacancies or interstitials (point defects) occurred in the 700 °C-annealed β-$Ga_2O_3$. However, the 800 °C-annealed samples exhibited 1.25% net Ga vacancies (or 0.83% O interstitials), while the as-grown and 900 °C-annealed samples exhibited 4.75% and 6% net O vacancies (or 3.17% and 4% Ga interstitials), respectively. Ga vacancies and O interstitials behave as effective positive ions (cations) and O vacancies and Ga interstitials behave as effective negative ions (anions) [26, 27]. Studies have found that anion-cation pair defects (Frenkel pairs) occur in vacancies and interstitials in β-$Ga_2O_3$ [28–30]. These defects cannot be detected by using the net atomic composition [31].

**Table 1. Comparison of Atomic Composition of As-grown and Post-annealed β-$Ga_xO_{1-x}$ Epilayers Studied by an RBS Technique**

| Sample | Ga (%) | O (%) |
|---|---|---|
| As-grown | 41.9 | 58.1 |
| 700 °C-annealed | 40.0 | 60.0 |
| 800 °C-annealed | 39.5 | 60.5 |
| 900 °C-annealed | 42.4 | 57.6 |

### *3.6 Time-dependent photoresponsivity*

Figures 6(a)–6(d) show a comparative analysis of the response and recovery times of different PDs. The photocurrent for a PD based on as-grown β-$Ga_2O_3$ in Fig. 6(a), increases rapidly from approximately 3 nA of dark current to a non-stable value of approximately 2.5 μA when illumination is on. However, the recovery time was extremely slow when the light was off. Electron-hole trapping states that prevent charge-carrier recombination may cause the slow recovery time. During the 60s periodic illumination switching, a low photo-dark current ratio of 1 order of magnitude was obtained.

#196199 - $15.00 USD Received 21 Aug 2013; revised 27 Sep 2013; accepted 30 Sep 2013; published 7 Oct 2013

Figure 6(b) show the time-dependent photoresponsivity of a PD based on a 700 °C-annealed sample. The dark current was approximately 4 pA, which is extremely low and favorable for practical detectors. When illuminated, the photocurrent instantaneously increased by approximately 5 orders of magnitude to a stable value of approximately 0.4 μA. The recovery time when illumination was off was rapid. This performance is inordinately better than that of the as-grown samples and is also comparable with the best PDs [32, 33]. HR-XRD rocking curves showed better crystallinity for the as-grown sample than the 700 °C-annealed sample. Additionally, cross-sectional FE-SEM images show more fractures along the extended grains in 700 °C-annealed samples than in as-grown samples, therefore this significant difference in their time-dependent photoresponsivity must be caused by the higher point defect density in as-grown β-$Ga_2O_3$ epilayers. These results indicate that functional time-dependent photoresponsivity of PDs is more sensitive to point defects than crystallinity.

Figure 6(c) shows the time-dependent photoresponsivity of a PD based on an 800 °C-annealed sample, with a dark current of approximately 70 pA. On illumination, the photocurrent rapidly increased by approximately 4.5 orders of magnitude to approximately 10 μA. When the light was off, the photocurrent suddenly decreased to 20 nA, decaying slowly and exponentially. This PD performed worse than the 700 °C-annealed sample. Figure 6(c) reflects a weaker performance than Fig. 6(b) because cross-sectional FE-SEM revealed more crystalline damage or because of the point defects calculated in the RBS analysis. HR-XRD rocking curves showed a better crystallinity for the 800 °C-annealed sample than the 700 °C-annealed sample. But, time-dependent photoresponsivity results indicate on non-reliability of synchrotron HR-XRD technique, which has a high accuracy, to choose a high quality sample for PD applications. Samples with lower degree of crystallinity, measured by a synchrotron HR-XRD technique, may have the highest quality for PD applications.

A dark current of approximately 0.3 nA and a photo-dark current ratio of approximately 4 orders of magnitude were obtained for a typical PD based on a 900 °C-annealed sample, as shown in Fig. 6(d). FE-SEM results show that the 900 °C-annealed samples produced larger fractures than the 800 °C-annealed samples, minimizing the role of high crystallinity in time-dependent photoresponsivity. As shown in Fig. 6(d), when illumination was off, the current rapidly decreased to approximately 40 μA and then gradually decayed.

### *3.7 Point defects mechanisms in photoresponsivity*

The RBS data showed the net vacancy of the as-grown sample is more than that of 800 °C-annealed sample and less than that of 900 °C-annealed sample. However, time-dependent photoresponsivity shows that PDs based on as-grown samples was extremely different to PDs based on the other samples. Additionally, HR-TEM image showed a high density of pair point defects in the as-grown samples. The schematic diagram of defect dynamics in reaction with the illuminated light may help understanding the unusual delay in the recovery time of the PD based on the as-grown sample.

#196199 - $15.00 USD Received 21 Aug 2013; revised 27 Sep 2013; accepted 30 Sep 2013; published 7 Oct 2013

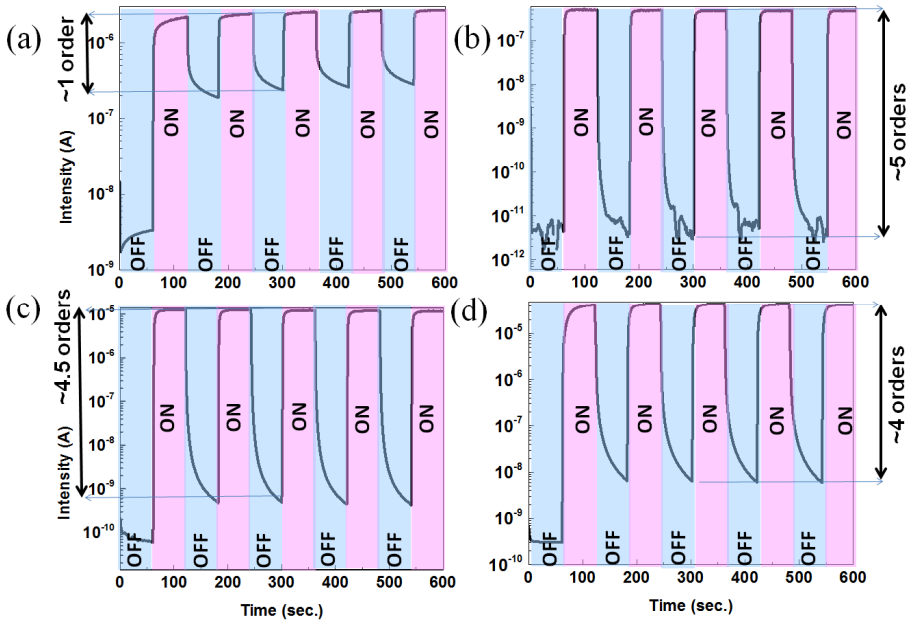


Fig. 6. Time-dependent photoresponsivity of typical PDs based on (a) as-grown, (b) 700 °C, (c) 800 °C, and (d) 900 °C-annealed β-$Ga_2O_3$.

Figures 7(a)–7(d) show the various time-dependent photoresponsivity processes of a PD based on an epilayer. The photo-generation process of electron-hole pairs during light illumination is shown in Fig. 7(a). Electrons and holes accelerate toward positive and negative electrodes, respectively, with applied voltage (Fig. 7(b)). Cations trap electrons and anions trap holes. The defects, in the form of cation-anion pairs, in Fig. 7(c) trap electron-hole pairs. The cation-anion pairs delay the time-dependent photoresponsivity of PDs because they disturb the charge collection toward positive and negative electrodes. Trapping centers, which are current leakage sources, delay the response and recovery times of optoelectronic devices. Figure 7(d) shows the simultaneous presence of net point defects (cations) and cation-anion pairs. Untrapped electron-hole pairs can move freely toward opposite charged electrodes, but, trapped electron-hole pairs delay current generation. Both photo-generated electron-hole pairs are trapped in cation-anion pair defects, but cation or anion net defects only trap electrons or holes. Untrapped holes or electrons may release their pairs. Figure 7(d) shows how some free holes may be attracted toward the electrons trapped by the net cation defects, and release them. Therefore, cation-anion pair defects, which are found in HR-TEM images of the as-grown β-$Ga_2O_3$ samples, contribute much more than net vacancies, measured by RBS technique, to current leakage.

#196199 - $15.00 USD Received 21 Aug 2013; revised 27 Sep 2013; accepted 30 Sep 2013; published 7 Oct 2013

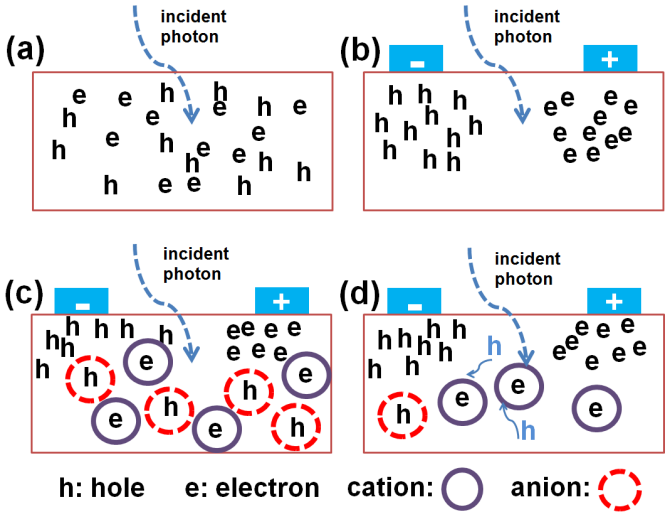


Fig. 7. Schematic diagrams of photo-generated electron-hole pairs in the (a) absence and (b) presence of applied voltage. Schematic diagrams of photo-generated electron-hole pairs under an applied voltage in the presence of (c) cation-anion pair defects and (d) cation-anion pair defects along with net cation defects.

*3.8 CL*

Figure 8(a) shows normalized CL spectra of all β-$Ga_2O_3$ samples, allowing the positions of the two main peaks and their shoulders from each sample to be compared. Figure 8(b) shows the original CL spectra (before normalization), which can be used for an intensity comparison. The first main peaks located in the higher energy region are attributed to β-$Ga_2O_3$ near band edge [34] (NBE) emissions. The NBE peak of the as-grown sample covers a wavelength region from 233 nm to 294 nm. The NBE emission regions of the 700 °C and 800 °C-annealed samples are the same (from 228 nm to 296 nm). It shifted from 210 nm to 290 nm for the 900 °C-annealed sample. The first 3 samples produced similar NBE emission regions. The NBE emission region shifted considerably toward a higher energy region for the 900 °C samples. The dominant crystallinity plane changed from (–402) for first 3 samples to (401) for the last sample, suggesting that the NBE emission region is a function of the dominant crystalline plane structure. The small shoulders on the NBE peaks of the first 3 and last samples were centered about 258 nm, 238 nm, 238 nm, and 218 nm, respectively. These shoulders may be caused by point defects, dislocations, surface states, phase impurities, or an unknown phenomenon.

The second largest peaks, called deep level (DL) peaks, in all the samples were broader with higher intensities than the NBE peaks. DL peaks are usually attributed to the presence of external and internal point defects or lattice defects [34]. A simple comparison between NBE emissions and DL peaks suggests that if broad and vigorous peaks arise from external impurities, the ratio of impurities to the original β-$Ga_2O_3$ atomic compounds is significant. However, the synchrotron HR-XRD and RBS results did not reflect any considerable external structures or impurities. Moreover, the net vacancies and interstitials ratio compared to the original atomic constitutive of β-$Ga_2O_3$ is not remarkable. Therefore, the broad peaks cannot be a main or direct function of internal or external point defects. The comparison between the CL spectra of the as-grown and post-annealed samples supports this hypothesis.

The PD and HR-TEM data showed that, as-grown samples exhibit the highest density of cation-anion pair defects, many of which are repaired during post-annealing. However, as shown in Fig. 8(b), the only absent peak after post-annealing is a low-intensity shoulder in the ultraviolet region centered about 329 nm. However, the intensity of the main DL peak increased for the 700 °C and 800 °C-annealed samples. PD data indicates that the number of

#196199 - $15.00 USD Received 21 Aug 2013; revised 27 Sep 2013; accepted 30 Sep 2013; published 7 Oct 2013

point defects decreased considerably in the 700 °C and the 800 °C-annealed samples. Cross-sectional FE-SEM results reflect the higher number density of crystalline damages in these samples. This investigation did not find evidence of the direct considerable participation of point defects in the form of vacancies or interstitials in the CL properties of β-$Ga_2O_3$. This indicates that crystalline damages affect DL emissions. The NBE and DL peak increases of the 900 °C-annealed samples may be a function of crystalline structure along with fractures. Unlike the PD results, CL spectroscopy assesses the quality of the as-grown samples based on their applications in deep ultraviolet regions. Therefore, low intensity DL peak of a CL spectrum of an epilayer does not necessarily indicate its good quality for PD applications.

For the 700 °C and 800 °C-annealed samples, with the same crystalline structure, increasing the post-annealing temperature shifted the maxima intensity of the DL peaks to the higher energy region. Crystalline damage may affect shifting the DL maximum toward the higher energy region. This shift toward a higher energy region is much higher for the 900 °C-annealed sample. This may be because it was re-crystallized in another preferred direction.

The shoulder position in Fig. 8(b) centered on 490 nm was fixed for all samples. The shoulder of the as-grown sample possesses the highest intensity of its CL spectrum. The shoulder of the 900 °C-annealed sample is very small compared to the other regions of the spectrum. Surface states on metal oxides are called common defects because of the presence of unsaturated atomic bonds at their surfaces. The oxygen atoms in the free air are adsorbed by the unsaturated atomic bonding at the surface, creating small p-n junctions [35] which may cause these shoulders. The surface states density in the as-grown samples is high, which decreases during post-annealing at 700 °C and 800 °C. During re-crystallization of the samples at 900 °C, a new opportunity may occur for the surface atomic bonds to rearrange themselves, decreasing the surface states effects. Surface p-n junctions are composed of a few atoms, creating a gradient in the crystalline structure immediately beneath the surface. Therefore, these p-n junctions do not exhibit crystalline structures. Before and after post-annealing the effect of these p-n junctions on the structural property of the materials is fixed, which may explain their fixed positions in the CL spectra.

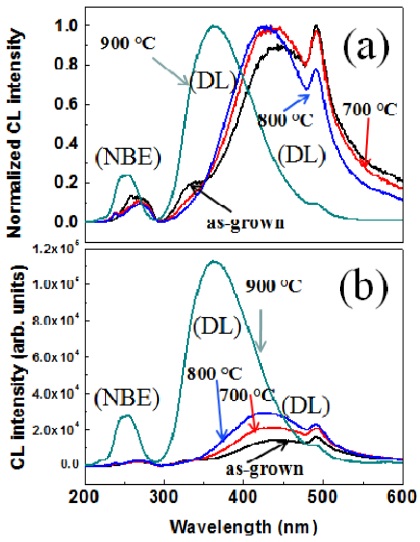


Fig. 8. Room temperature cathodoluminescence (CL) spectra of as-grown and post-annealed β-$Ga_2O_3$ at 700 °C, 800 °C, and 900 °C (a) after normalization for peak position comparison and (b) before normalization for peak intensity comparison.

#196199 - $15.00 USD Received 21 Aug 2013; revised 27 Sep 2013; accepted 30 Sep 2013; published 7 Oct 2013

## 4. Conclusion

This study examines the effects of crystallinity and point defects on the time-dependent photoresponsivity and CL properties of β-$Ga_2O_3$ epilayers. Synchrotron HR-XRD shows the same crystalline structure with a dominant orientation of (−402) for the as-grown and 700 °C and 800 °C-annealed samples. The dominant orientation converts to (401) for the 900 °C-annealed samples. As-grown samples show the highest crystallinity. Cross-sectional FE-SEM images show that samples treated at higher post-annealing temperatures exhibit more fractures. HR-TEM images show a high density of Frenkel pairs in the as-grown samples. Point defects affect the time-dependent photoresponsivity of β-$Ga_2O_3$ epilayers more than crystallinity. The recovery time for PDs based on as-grown β-$Ga_2O_3$ epilayers is slow, but extremely fast for the post-annealed samples. Post-annealing provides sufficient energy for the cation-anion pair defects in the as-grown samples to repair each other. Of all the devices, PDs based on 700 °C-annealed β-$Ga_2O_3$ epilayers produce the lowest dark current (approximately 70 pA) and the highest photo-dark current ratio (approximately 5 orders of magnitude). These results show that 700 °C-annealed β-$Ga_2O_3$ epilayers are some of the best materials for optoelectronic devices that are sensitive to fast time-dependent photoresponsivity. Unlike time-dependent photoresponsivity, crystalline structure and fractures affect the origin and intensity of DL peaks in CL spectra of β-$Ga_2O_3$ epilayers more than point defects. Point defects may produce the different shoulders in the NBE and DL peaks of the CL spectra. This confirms hypotheses on the effect of crystalline damage of materials on their CL properties.

## Acknowledgments

This work is supported by the National Science Council of Taiwan under grant nos. NSC-100-2221-E-005-092-MY3 and 102-2218-E-005-001, by Ministry of Economic Affairs under contract no. 100-EC-17-A-07-SI-158, and by the Southern Taiwan Science Park under contract no. 102CE06. We acknowledge Y. F. Lai from NCHU for FE-SEM samples preparation.